Journal of Medicinal Chemistry

Article

Cite This: J. Med. Chem. 2018, 61, 2292−2302

pubs.acs.org/jmc

Introduction of Intrinsic Kinetics of Protein−Ligand Interactions and Their Implications for Drug Design

Vaida Linkuvienė,[†,∥] Vladimir O. Talibov,[‡,∥] U. Helena Danielson,[‡,§] and Daumantas Matulis*[,†]

[†]Department of Biothermodynamics and Drug Design, Institute of Biotechnology, Vilnius University, Saulėtekio 7, Vilnius, LT-10257, Lithuania

[‡]Department of Chemistry - BMC, Uppsala University, Box 576, Uppsala, SE-751 23, Sweden

[§]Science for Life Laboratory, Uppsala University, Uppsala, SE-751 23, Sweden

Supporting Information

ABSTRACT: Structure−kinetic relationship analyses and identification of dominating interactions for optimization of lead compounds should ideally be based on *intrinsic* rate constants instead of the more easily accessible *observed* kinetic constants, which also account for binding-linked reactions. The intrinsic rate constants for sulfonamide inhibitors and pharmacologically relevant isoforms of carbonic anhydrase were determined by a novel surface plasmon resonance (SPR) biosensor-based approach, using chemodynamic analysis of binding-linked pH-dependent effects. The observed association rates (k_a^{obs}) were pH-dependent and correlated with the fraction of deprotonated inhibitor and protonated zinc-bound water molecule. The intrinsic association rate constants (k_a^{intr}) were pH independent and higher than k_a^{obs}. By contrast, the observed and intrinsic dissociation rate constants were identical and pH-independent, demonstrating that the observed association and dissociation mechanisms are inherently different. A model accounting for the differences between intrinsic and observed rate constants was developed, useful also for other interactions with binding-linked protonation reactions.

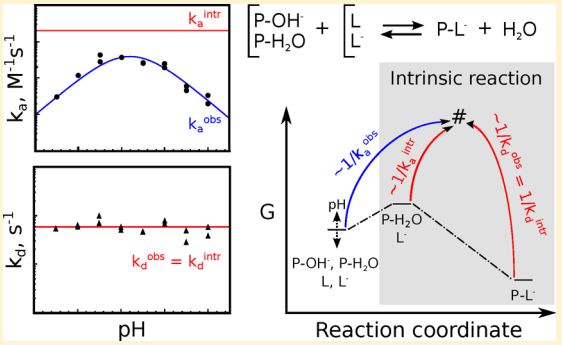

INTRODUCTION

Rational drug design involves the determination of the kinetics of the interactions between the lead compound and the target protein. The association and dissociation rate constants (k_a and k_d) and the thermodynamic equilibrium dissociation constant (K_D) of the interaction are all important for judging the suitability of a compound to be developed as drug, and how it should be optimized. However, most ligand−protein interactions involve various binding-linked reactions, typically protonation of the protein or ligand, or binding-linked conformation changes of the protein or the ligand. Here we show that such reactions may reduce the *observed* constants (k_a^{obs} and k_d^{obs}) and significantly affect the results and the interpretation of structure−activity relationships. It is important to eliminate all such binding-linked reactions via a proper analysis and to estimate the *intrinsic* constants (k_a^{intr} and k_d^{intr}). These may be used to more precisely explain how ligand structure affects the interaction and which routes for structural optimization should be followed for the development of the compound.

Carbonic anhydrase (CA) represents a large family of enzymes. It catalyzes the hydration of carbon dioxide to form bicarbonate while releasing a proton, via a mechanism involving a prosthetic Zn^{2+} ion that coordinates the water molecule.[1,2] This reaction is important for carbon metabolism, pH homeostasis, and numerous physiological processes. There are 15 highly homologous α-CA isoforms in humans, of which 12 are catalytically active and 3 are inactive. The isoforms differ in their activity and cellular/tissue localization. The decrease or increase of CA activities in a tissue may lead to numerous pathological conditions. CAs are thus targets for numerous pathologies, with glaucoma being the primary disease treated with CA inhibitors today. However, several isoforms are emerging as potential cancer targets; for example, membrane-bound CA IX, which has an increased expression in tumor cells under hypoxic conditions and is now considered to be both a good tumor marker and a target for anticancer therapy.[2−4]

Substituted aromatic sulfonamides (SAs) are well-known CA inhibitors. They may bind with extraordinary high (picomolar) affinities and exhibit significant selectivity toward a particular CA isoform.[5] Since the first demonstration that sulfonamide binding is pH-dependent and protonation-linked,[6] and the demonstration by neutron diffraction that acetazolamide is bound to CA II in the deprotonated form,[7] it is generally believed that sulfonamide compounds bind to the prosthetic zinc atom in the active site with the sulfonamide amino functional group in the deprotonated, negatively charged form, and that the water bound to the active site Zn^{2+} is in a protonated state, favoring its substitution from the zinc coordination sphere by the sulfonamide. However, an alternative mechanism has been postulated.[8]

Received: September 28, 2017
Published: February 21, 2018

DOI: 10.1021/acs.jmedchem.7b01408
J. Med. Chem. 2018, 61, 2292−2302

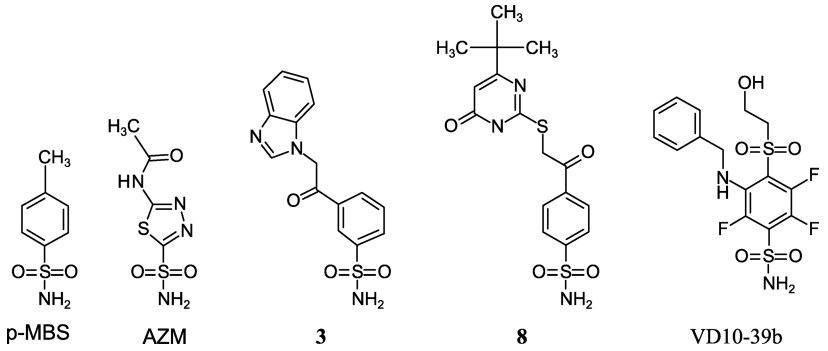

Figure 1. Structures of CA inhibitors analyzed in the present study to determine the intrinsic interaction rates from SPR data obtained at various pH.

It assumes a linked protonation−deprotonation event between the amide group of the ligand and a zinc-coordinated hydroxide directly in the active site of the enzyme, after the formation of an encounter complex. An additional uncertainty with respect to the fundamental interaction mechanism is the observation that association rates for sulfonamides are relatively slow,[9] which is unexpected considering that association is driven by a strong electrostatic interaction between the negatively charged sulfonamide and the positively charged Zn^{2+}. Resolving the mechanism of sulfonamide inhibitors is of importance for the design of *specific* inhibitors, as different isozymes have different pK_a of the Zn^{2+}-coordinated water molecule in the active site. Moreover, they are associated with different pathologic conditions, potentially motivating different pH-dependencies for different isoenzymes. The design of compounds efficient in a physiological environment should therefore also account for effects of varying pH.

To better understand the interaction mechanism and its pH dependency, we have here exploited our previous observation that it is possible to determine the intrinsic binding thermodynamic constants for CA inhibitors by analyzing the pH-dependency of these interactions[10−16] and, for the first time here, determine the intrinsic rate constants by using surface plasmon resonance (SPR) biosensor technology. Although SPR-based kinetic analysis of interactions between drug-like compounds and target proteins has become a key method for drug discovery, and has been a subject of several reviews,[17−20] it is yet not used to its full potential for characterizing the details of molecular interactions. The determined k_a and k_d rate constants provide important information about interaction mechanisms and inhibitor properties, allowing the rational modification of compounds and optimization of their binding characteristics. However, typical SPR experiments provide *observed* kinetic parameters rather than *intrinsic* kinetic parameters, which are independent of complexities such as protonation-linked reactions.

This study was based on the determination of the kinetic parameters for a series of aromatic sulfonamide inhibitors, varying in the position and size of the aromatic substituent (Figure 1), and three CA isoforms (CA II, IX, and XIII). Corresponding data could subsequently be calculated for an additional three isoforms (CA I, VII, and XII) and various ligands for which observed interaction kinetic parameters have been previously determined.[9] This enabled a structure-intrinsic kinetic relationship analysis, also comparing effects on different isoforms. This analysis confirmed that the intrinsic rate constants were significantly faster than the observed rate constants, for all inhibitors and isozymes, which is consistent with a mechanism involving the deprotonation of the inhibitor before binding to the protonated zinc-bound water molecule. The adopted approach is novel and allows for an improved understanding of how inhibitors can be optimized for potency and specificity, essential for development of efficient and safe drugs targeting not only the specific members of the CA family, but should be applicable to any ligand−protein interaction where linked protonation reactions occur.

RESULTS

Model for Sulfonamide Interactions with Carbonic Anhydrase. To rationalize the difference between the observed and intrinsic rate constants and the pH dependence of the kinetic parameters for sulfonamides interacting with carbonic anhydrase, we developed a mechanistic model (Figure 2). The molecular species that occur and account for the observed interaction are indicated in the top scheme (A), while those involved in the intrinsic interaction, and their prereaction interconversions, are specified below (B). This model assumes that sulfonamides are in the deprotonated, anionic form when they interact with the Zn^{2+} cation in the active site of the carbonic anhydrase, and that the water molecule occupying the fourth coordination space of the metal ion has to be in a protonated, electrostatically neutral form in order to be substituted by the deprotonated sulfonamide. Depending on the pH, two reactions may consequently have to occur before the ligand can interact with the active site Zn^{2+}: (1) protonation of the Zn^{2+}-bound hydroxide (top, black), and (2) deprotonation of the sulfonamide (bottom, red).

As previously shown for the fraction of active species dependence on pH,[21,22] the fraction of CA bearing a protonated water molecule in its active site (f^{CA}) can be described by eq 1 and estimated if the pK_a of the coordinating water molecule (pK_a^{CA}) is known:

$$f^{CA} = \frac{10^{pK_a^{CA}-pH}}{1 + 10^{pK_a^{CA}-pH}} \quad (1)$$

Similarly, the fraction of inhibitor in the deprotonated form (f^{SA}) can be described by eq 2 and estimated if the pK_a of the sulfonamide group (pK_a^{SA}) is known:

$$f^{SA} = \frac{10^{pH-pK_a^{SA}}}{1 + 10^{pH-pK_a^{SA}}} \quad (2)$$

These equations were used to visualize how the fraction of the reactants vary with pH (Figure 2C). The graph illustrates that the fraction of binding competent CA is lower above the pK_a, which for most CA isoforms is in the near-neutral pH range. The opposite relationship applies to the sulfonamides, which have a higher fraction of the binding competent form at pH values above their near neutral pK_a. The pK_a values of CA isoforms and sulfonamide compounds used in this study were taken from[10,15,16,23−29]

DOI: 10.1021/acs.jmedchem.7b01408
J. Med. Chem. 2018, 61, 2292−2302

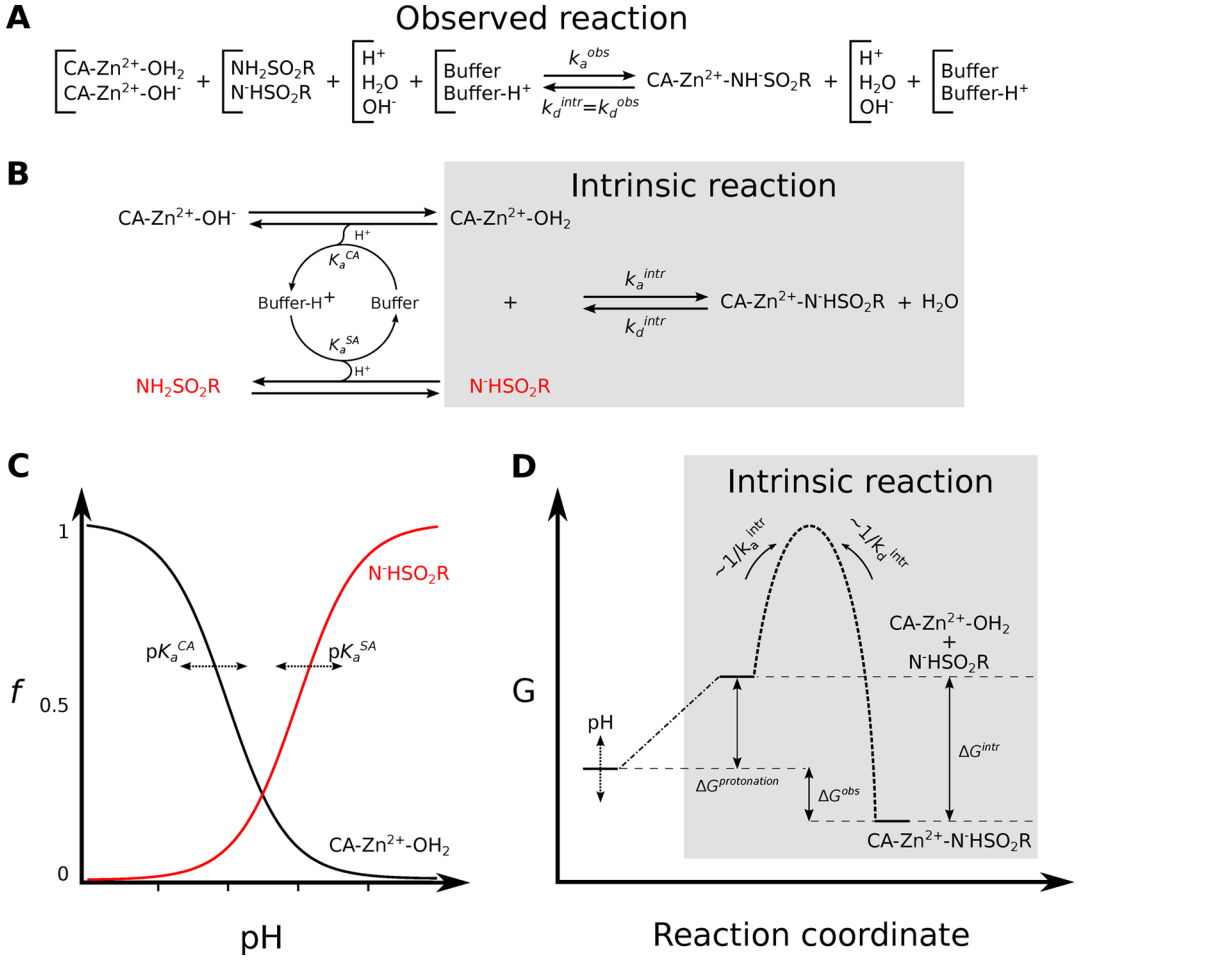

Figure 2. Mechanistic principles for an interaction between a sulfonamide inhibitor and a carbonic anhydrase. (A) Scheme for the observed reaction and the molecular species involved. (B) Scheme for the intrinsic reaction (shaded in gray) and the molecular species involved. (C) pH-dependencies of the concentrations of protonated CA active site (black) and deprotonated sulfonamide (red); mathematical expressions are given in eqs 1 and 2, respectively. (D) Free energy (G) profile for the observed and the intrinsic reactions.

The binding of sulfonamides to CA is expected to be optimal at near-neutral pH, as the charges on the interacting groups are unfavorable in both acidic and alkaline environments. To translate this structural information into terms of kinetics and affinity, we modified the standard reversible second-order rate equation.

The observed association rate is a function of the intrinsic association rate and the available fractional concentrations of the interacting species:

$$k_a^{obs} = k_a^{intr} f^{CA} f^{SA} \quad (3)$$

The intrinsic association constant k_a^{intr} can thus be expressed as a function of the observed association constant and the fraction of binding-competent forms:

$$k_a^{intr} = \frac{k_a^{obs}}{f^{CA} f^{SA}} \quad (4)$$

The fractional concentration of the associating species is pH-dependent but opposite (Figure 2C). As the exact lateral position of two curves depend on the pK_a's of the sulfonamide and the Zn^{2+}-bound water molecule, the exact pH for the optimum is a characteristic for both the specific inhibitor and the CA isoform.

Furthermore, the model assumes that the observed and intrinsic dissociation rates are equal and essentially pH independent as they both involve a simple dissociation of the ligand−target complex:

$$k_d^{obs} = k_d^{intr} \quad (5)$$

Taken together, these equations can be used to define affinities and their pH dependencies, as the intrinsic equilibrium dissociation constant (K_D^{intr}) is equal to the ratio of dissociation and association rate constants:

$$K_D^{intr} = \frac{k_d^{intr}}{k_a^{intr}} \quad (6)$$

This is illustrated in the free energy diagram (Figure 2D), which also shows the kinetic barrier of association and dissociation and why the observed rate of association and affinities vary with pH, while the rate of dissociation is pH insensitive. The scheme (Figure 2D) illustrates that the observed and intrinsic rates may be quite different and depend on pH.

pH-Effects on Intrinsic and Observed Interaction Kinetics. SPR biosensor surfaces were generated by immobilizing proteins to levels suitable for quantifying interactions with the selected set of ligands and using buffers spanning a wide pH range. Interaction experiments were subsequently performed at pH values ranging from 5.5 to 9 for a set of inhibitors and CA II, CA IX, and CA XIII. Representative sensorgrams are shown

DOI: 10.1021/acs.jmedchem.7b01408
J. Med. Chem. 2018, 61, 2292−2302

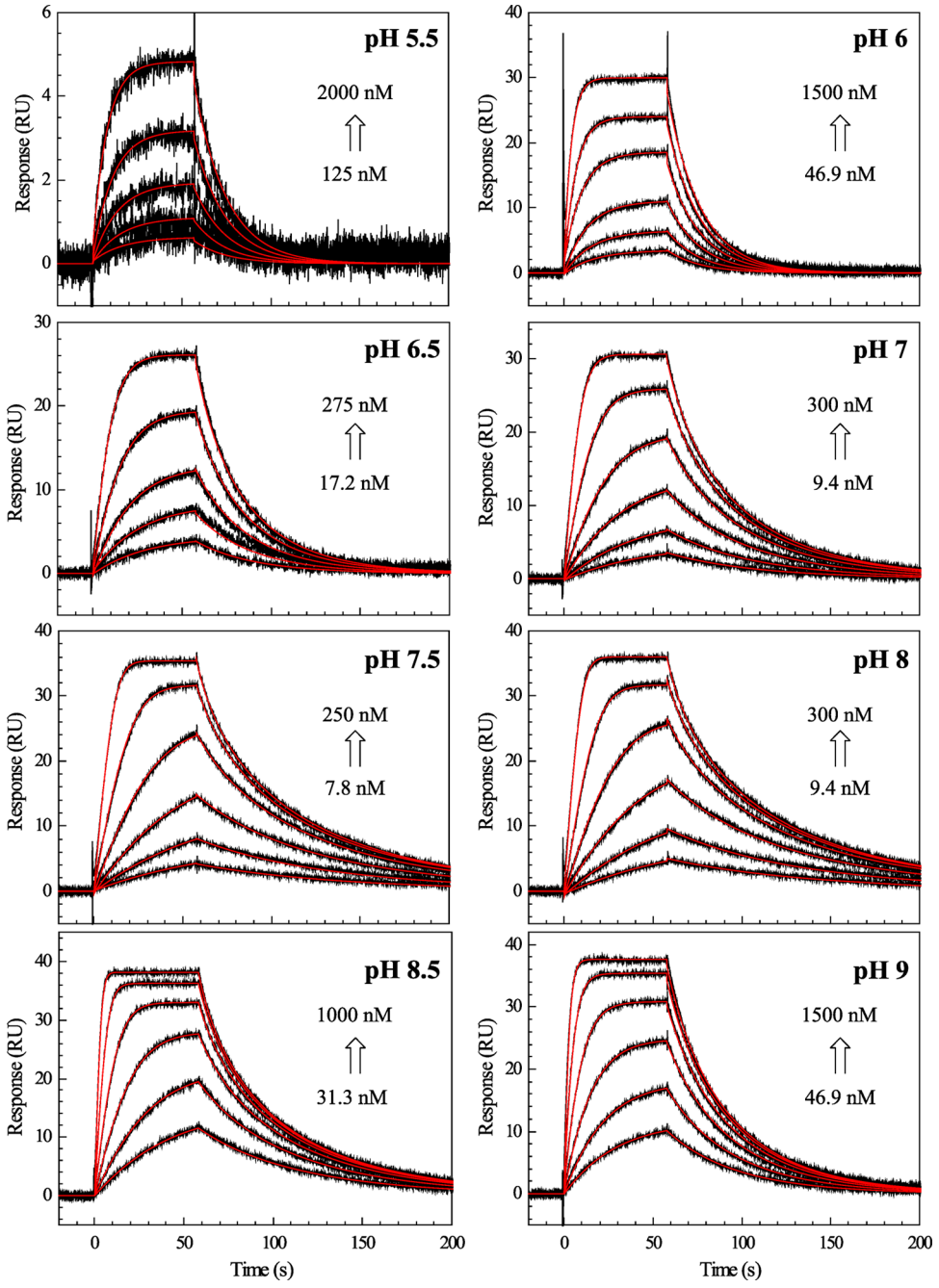

Figure 3. Sensorgrams for interactions between VD10-39b and immobilized CA II at pH from 5.5 to 9. The compound was injected in a 2-fold dilution series, starting at a concentration estimated to be 10 times the expected K_D. The concentration range is specified for each data set. Running buffers were adjusted to the indicated pH. Red lines represent best fit curves from nonlinear regression analysis, using a reversible 1:1 interaction model.

in Figure 3. The kinetic rate constants for k_a and k_d, and the equilibrium dissociation constant (K_D) at each pH were determined by global analysis of sensorgrams for a series of inhibitor concentrations (Table 1).

The protonation effect on the kinetics of protein−ligand interactions was demonstrated by analyzing the interaction between the selected ligands and CA II, CA IX, and CA XIII as a function of pH. Figure 4 demonstrates the dependency of observed kinetic parameters for the interaction between AZM and three different CA enzymes, and their rationalization using the model described above. The top panels illustrate that the observed association rate constants k_a are clearly pH-dependent, with an optimum around 7. In contrast, the observed dissociation rate k_d for CA II and CA XIII were essentially pH independent, while it increased slightly with pH for CA IX, within the experimental error (middle panels). Consequently, the equilibrium dissociation constants were pH-dependent, with a minimum around 7 for CA II and CA XIII (bottom panels). The K_D for CA IX was low for pH up to around 7, above which it increased linearly. As a reference, the corresponding equilibrium data determined by the fluorecent thermal shift assay (FTSA) is included for CA II, confirming that the two techniques give equivalent results.

Intrinsic versus Observed Kinetics. The observed kinetic parameters of structurally related compounds binding to 6 CA isoforms have previously been determined at physiological pH 7.4 and at several pH values for CA IX and XII, giving a qualitative

DOI: 10.1021/acs.jmedchem.7b01408
J. Med. Chem. 2018, 61, 2292−2302

Table 1. Observed Kinetic Rate Constants (k_a^{obs} and k_d^{obs}) and Thermodynamic Equilibrium Constants (K_D^{obs}) Determined at pH 7.0 while the Equivalent Intrinsic Parameters (k_a^{intr}, k_d^{intr}, K_D^{intr}) Were Quantified Using Eqs 4, 5, and 6[a]

		observed			intrinsic		
compound	isozyme	k_a^{obs}, M^{-1} s^{-1}	k_d^{obs}, s^{-1}	K_D^{obs}, M	k_a^{intr}, M^{-1} s^{-1}	k_d^{intr}, s^{-1}	K_D^{intr}, M
p-MBS	CA II	1.4×10^5	0.06	4.3×10^{-7}	4.5×10^8	0.06	1.3×10^{-10}
AZM	CA II	3.7×10^6	0.07	1.5×10^{-8}	2.2×10^7	0.06	2.6×10^{-9}
	CA IX	3.4×10^6	0.03	8.5×10^{-9}	2.8×10^7	0.03	1×10^{-9}
	CA XIII	4.1×10^5	0.015	3.65×10^{-8}	1.5×10^6	0.015	1×10^{-8}
VD10-39b	CA II	7.9×10^5	0.05	6.1×10^{-8}	2.2×10^7	0.044	2×10^{-9}
	CA XIII	1.3×10^6	0.015	1.2×10^{-8}	1.4×10^7	0.013	1×10^{-9}
8	CA II	8.1×10^5	0.04	5.14×10^{-8}	2×10^8	0.04	1.9×10^{-10}
	CA IX	2.5×10^6	0.1	4.2×10^{-8}	9×10^8	0.074	8×10^{-11}
3	CA IX	7.6×10^5	0.4	5.2×10^{-7}	7.5×10^8	0.4	1.3×10^{-9}
	CA XIII	7.3×10^4	0.08	1.2×10^{-6}	3.5×10^7	0.08	2.3×10^{-9}

[a]The table lists values from one experiment, while a complete set of rate constants for each compound at each studied pH, averaged from two or three independent experiments, is given in the Supporting Information.

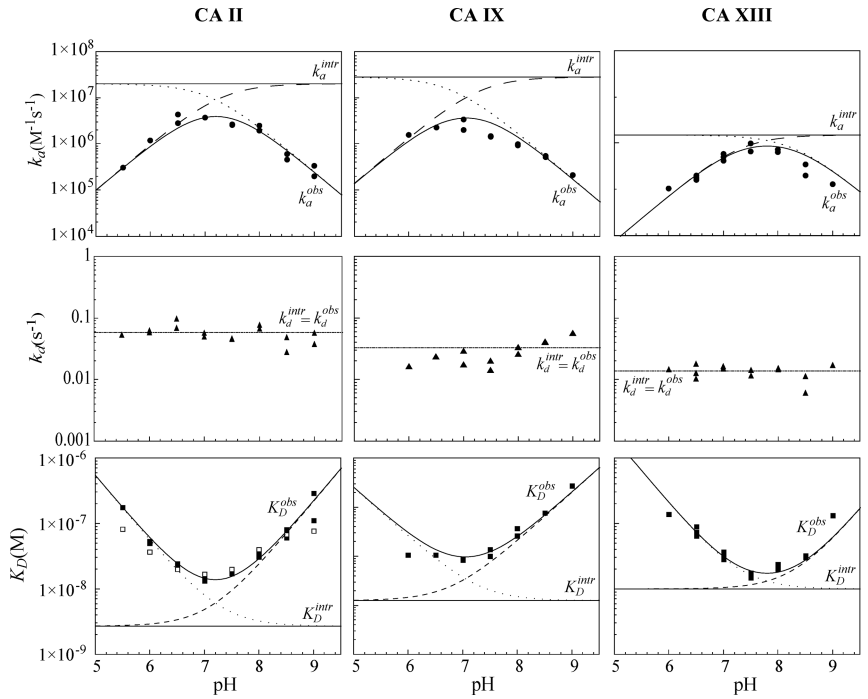

Figure 4. Observed kinetic and equilibrium data as a function of pH and the intrinsic values that are independent of pH. The kinetic parameters for AZM interaction with CA II, CA IX, and CA XIII were determined by SPR (solid symbols). K_D values, obtained by FTSA for the CA II–AZM interaction at various pH are included as open squares in the left bottom panel. Protein pK_a's were taken from refs 10, 15, 16. The dashed and dotted lines show the fractions of deprotonated sulofnamide and protonated CA, respectively.

insight on the fine details of the interactions.[9] Here we quantified the intrinsic kinetic parameters for CA II, CA IX, and CA XIII using the chemodynamic approach, i.e., by varying the pH and thereby the actual concentration of the reactive species. Furthermore, here we calculate intrinsic kinetics of previously measured compound interaction.[9]

Figure 5 compares the intrinsic and observed thermodynamic parameters of the fluorinated compounds interaction with five CA isoforms. Unfortunately, the most tightly binding compounds exhibited rates of dissociation that were too slow to be determined by SPR in a given experimental set up. Generally, biosensor analysis with slow dissociating inhibitors requires single-cycle kinetics experiments[30] or prolonged dissociation phases, unless surface regeneration can be implemented. Therefore, evaluation of a set of tight binders toward multiple targets becomes challenging. Even in the absence of rebinding events and any mass-transport reactions involved,[31] the half-life of a complex with the dissociation rate constant of $1 \times 10^{-3} s^{-1}$ exceeds 11 min. Here the kinetic parameters for such stable interactions were estimated by multiplying the approximate association rates determined by SPR by the K_D values previously determined by the thermal shift assay, as a good correlation between these methods has been shown before.[9] They are found in the gray shaded area of the graph with very slow dissociation rates. The intrinsic association rate constants were 1 to 2 orders of magnitude greater than the observed ones, with slight differences depending on the pK_a's of the compound and the CA isoform. However, the intrinsic dissociation rate constants were the same as observed ones. It is clear that the rates are highly dependent both on the structure of the compound and on the microenvironment in the active site of the CA paralogue.

All intrinsic association rate constants (Figure 5) were between 3.3×10^5 and 8.8×10^8 M^{-1} s^{-1}, while the observed

DOI: 10.1021/acs.jmedchem.7b01408
J. Med. Chem. 2018, 61, 2292–2302

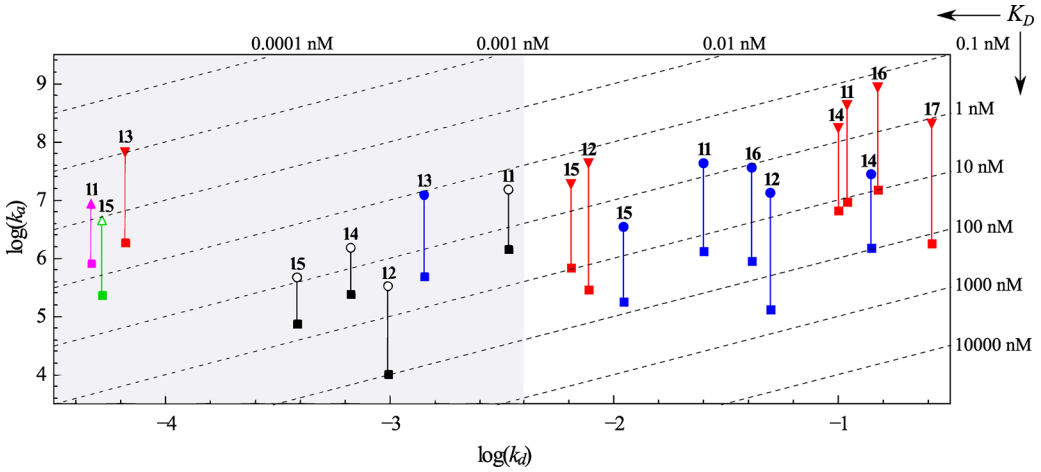

Figure 5. Comparison of observed (bottom squares) and intrinsic (upper shapes) kinetic parameters for sulfonamides **11**−**17** interacting with CA IX (red down-pointing triangle), CA XII (blue filled circles), CA I (magenta filled triangle), CA VII (green open triangle), and CA XIII (black open circle). Intrinsic and observed values for a certain interaction are connected by vertical lines. Interaction rate constants that could be determined directly by SPR are located on the right-hand half of the plot (unshaded), while rate constants determined approximately by SPR (k_a) and the corresponding k_d values estimated by multiplying the k_a's by K_D determined by thermal shift[9] are located on the left half of the plot (shaded).

rates varied between ~10^4 and 10^7 M^{-1} s^{-1}. The intrinsic dissociation rate constants spanned an even slightly greater interval, from 1.0×10^{-1} s^{-1} to 6.6×10^{-5} s^{-1} (equivalent to residence times from 10 s to 4.2 h). The tightest binder of CA IX, compound **13**, whose intrinsic thermodynamic dissociation constant K_D is equal to approximately 1 pM, is such a great binder of CA IX primarily due to its long residence time, while the association rate is not exceptional. Similarly, the high affinity between compound **11** and CA I, and between **15** and CA VII is exceptionally strong, primarily due to extremely long residence times. It should be noted that interactions in the right part of the figure (unshaded) have both association and dissociation rates, and the corresponding thermodynamic K_D, determined accurately and independently. By contrast, the parameters on the left shaded part of the figure are approximate since they were generated indirectly also using data from thermal shift experiments due to the lack of k_d measurements. However, the leftmost data points are of great interest because these compounds possess an exceptional stability in their interaction with certain CA isoforms.

Structure-Intrinsic Kinetic Relationship Analysis. To better understand the reasons behind the exceptional residence times of selected compounds, the correlations between intrinsic kinetic constants and the chemical structures of all compounds, both tested previously[9] and here, were analyzed. The intrinsic values of kinetic parameters for all CA isoforms, namely, CA I, CA II, CA VII, CA IX, CA XII, and CA XIII, and compounds **1** to **17** are listed in Table 2. The kinetic parameters of compounds with similar chemical structures are plotted in Figures 6 and 7.

Figure 6 compares the intrinsic kinetic binding parameters of compounds with and without an *ortho* chloro substitution. In panel A, for compound **1**, the Cl *ortho* substitution reduced the affinity toward all tested isoforms primarily due to slowing the association rate but also for most isoforms due to faster dissociation rate (CA VII, CA IX, and CA XII). Similar observations are shown in panels B−D, for *ortho* Cl addition to compounds **3**, **6**, and **9**.

Compounds **3**, **4**, and **5** had higher k_d values compared to compounds **1** and **2**. The fastest interaction occurred for compound **3** and CA IX. This compound associated rapidly with CA II and CA VII and dissociated fast from all studied CAs except CA XIII. Dissociation from CA XIII was the slowest of all 10 compounds, shown in Figure 6, with several exceptions, e.g., compound **5** dissociation from CA XII. The fastest association (k_a) and dissociation (k_d) rates were determined for the interaction between compound **6** and CA XII. Its analogue bearing chlorine **7** had lower affinity. Compounds with (**10**) and without (**9**) *ortho*-chlorine are compared in panel D, Figure 6. Compound **9** associated faster and dissociated slower from to CA IX compared to compound **10**. This tendency is illustrated in panels A, B and C, Figure 6.

Figure 7 shows the intrinsic kinetic parameters of the fluorinated compounds. Compounds **11** and **16** are *para*-substituted benzenesulfonamides, while the remaining compounds bear additional substitutions at *ortho*- or *meta*-positions that cause selectivities toward particular CA isoforms. Compound **17** does not possess any *para*-substitution and only an *ortho*-substitution. Figure 7 shows only the data where both the association and dissociation rates were accurately determined. The strongest binders with slow dissociation rates could not be determined and thus only some of them are shown in the shaded area of Figure 5, as explained above.

Addition of the octylamine *ortho*-substitution to compound **11** diminished both the association and dissociation rates, thus not affecting the affinity toward CA IX. However, FTSA data indicated that **12** bound stronger than **11**. This slight inconsistency is likely due to different measurement approaches, SPR requiring immobilization while FTSA involves heating. Still, the overall tendencies are the same in both techniques. Addition of *meta*-substitution of octylamine to compound **11**, resulting in compound **13**, caused significantly slower dissociation from CA IX as shown in the gray area of Figure 5.

DISCUSSION

Structure−kinetic and structure−thermodynamic relationships provide valuable information for structure-based drug design. In addition to standard biochemical assays, various biophysical techniques have emerged as orthogonal methods for screening, identification of, and optimization of leads.[32] By estimating thermodynamic parameters and kinetic constants, they can provide an in-depth understanding of the underlying interaction mechanisms and driving forces. However, the correlation between the physical parameters of an interaction and the target and ligand

DOI: 10.1021/acs.jmedchem.7b01408
J. Med. Chem. 2018, 61, 2292−2302

Table 2. Intrinsic Rate Constants of Association (k_a) and Dissociation (k_d) and the Intrinsic Thermodynamic Equilibrium Constants (K_D) for All Tested Compound Interaction with 6 CA Isoforms[a]

compound		CA I	CA II	CA VII	CA IX	CA XII	CA XIII
1	K_D, M	7.0×10^{-10}	-	3.8×10^{-11}	1.5×10^{-10}	1.0×10^{-9}	4.3×10^{-10}
	k_a, M^{-1} s^{-1}	1.1×10^{7}	-	1.5×10^{8}	4.1×10^{8}	5.0×10^{7}	1.3×10^{7}
	k_d, s^{-1}	7.9×10^{-3}	-	5.5×10^{-3}	5.9×10^{-2}	5.1×10^{-2}	5.7×10^{-3}
2	K_D, M	1.4×10^{-9}	1.3×10^{-10}	3.3×10^{-10}	6.0×10^{-10}	8.4×10^{-9}	1.9×10^{-10}
	k_a, M^{-1} s^{-1}	5.5×10^{6}	3.5×10^{7}	5.2×10^{7}	2.3×10^{8}	2.0×10^{7}	1.1×10^{7}
	k_d, s^{-1}	7.5×10^{-3}	4.6×10^{-3}	1.7×10^{-2}	1.4×10^{-1}	1.7×10^{-1}	2.0×10^{-3}
3	K_D, M	2.0×10^{-7}	1.3×10^{-9}	2.1×10^{-9}	1.3×10^{-9}	1.0×10^{-8}	2.3×10^{-9}
	k_a, M^{-1} s^{-1}	4.0×10^{6}	4.9×10^{8}	3.1×10^{8}	7.5×10^{8}	5.1×10^{7}	3.5×10^{7}
	k_d, s^{-1}	7.9×10^{-1}	6.2×10^{-1}	6.5×10^{-1}	4.0×10^{-1}	5.1×10^{-1}	8.0×10^{-2}
4	K_D, M	-	4.9×10^{-9}	1.3×10^{-8}	2.6×10^{-9}	6.8×10^{-9}	-
	k_a, M^{-1} s^{-1}	-	3.1×10^{7}	2.1×10^{7}	3.3×10^{8}	2.1×10^{7}	-
	k_d, s^{-1}	-	1.5×10^{-1}	2.7×10^{-1}	8.4×10^{-1}	1.4×10^{-1}	-
5	K_D, M	-	3.1×10^{-9}	2.4×10^{-9}	-	1.6×10^{-9}	1.3×10^{-8}
	k_a, M^{-1} s^{-1}	-	4.2×10^{7}	2.6×10^{7}	-	1.3×10^{7}	3.4×10^{6}
	k_d, s^{-1}	-	1.3×10^{-1}	6.1×10^{-2}	-	2.0×10^{-2}	4.3×10^{-2}
6	K_D, M	5.4×10^{-10}	1.7×10^{-11}	2.1×10^{-11}	1.3×10^{-10}	3.8×10^{-10}	5.3×10^{-10}
	k_a, M^{-1} s^{-1}	2.2×10^{7}	4.8×10^{8}	1.0×10^{9}	1.6×10^{9}	7.1×10^{9}	3.2×10^{7}
	k_d, s^{-1}	1.2×10^{-2}	8.0×10^{-3}	2.2×10^{-2}	2.1×10^{-1}	2.7	1.7×10^{-2}
7	K_D, M	7.6×10^{-10}	1.1×10^{-10}	1.0×10^{-10}	8.9×10^{-10}	1.8×10^{-9}	1.7×10^{-10}
	k_a, M^{-1} s^{-1}	1.1×10^{7}	3.8×10^{7}	4.2×10^{8}	2.9×10^{8}	1.8×10^{8}	2.6×10^{7}
	k_d, s^{-1}	8.4×10^{-3}	4.2×10^{-3}	4.6×10^{-3}	2.6×10^{-1}	3.2×10^{-1}	1×10^{-8}
8	K_D, M	3.8×10^{-11}	1.9×10^{-10}	2.3×10^{-10}	8.0×10^{-11}	2.8×10^{-10}	5.8×10^{-11}
	k_a, M^{-1} s^{-1}	4.4×10^{7}	2.0×10^{8}	1.1×10^{8}	9.0×10^{8}	9.0×10^{7}	1.7×10^{8}
	k_d, s^{-1}	1.7×10^{-3}	4.0×10^{-2}	1.0×10^{-2}	7.4×10^{-2}	2.5×10^{-2}	1×10^{-8}
9	K_D, M	6.8×10^{-9}	1.1×10^{-9}	3.9×10^{-9}	3.3×10^{-10}	-	4.0×10^{-9}
	k_a, M^{-1} s^{-1}	3.2×10^{7}	1.6×10^{8}	3.6×10^{8}	9.5×10^{8}	-	1.3×10^{7}
	k_d, s^{-1}	2.1×10^{-1}	1.8×10^{-1}	1.4	3.1×10^{-1}	-	5.1×10^{-2}
10	K_D, M	1.1×10^{-7}	1.5×10^{-9}	3.6×10^{-9}	1.4×10^{-9}	1.8×10^{-9}	5.6×10^{-9}
	k_a, M^{-1} s^{-1}	3.9×10^{6}	4.8×10^{7}	4.2×10^{7}	2.9×10^{8}	9.0×10^{7}	3.9×10^{6}
	k_d, s^{-1}	4.3×10^{-1}	7.3×10^{-2}	2.2×10^{-2}	4.0×10^{-1}	1.6×10^{-1}	1×10^{-8}
11	K_D, M	3.2×10^{-12}	-	1.9×10^{-10}	2.5×10^{-10}	5.8×10^{-10}	5.0×10^{-11}
	k_a, M^{-1} s^{-1}	8.5×10^{6}	-	1.7×10^{8}	4.4×10^{8}	4.3×10^{7}	1.5×10^{7}
	k_d, s^{-1}	2.7×10^{-5}	-	3.3×10^{-2}	1.1×10^{-1}	2.5×10^{-2}	7.6×10^{-4}
12	K_D, M	-	-	4.9×10^{-9}	1.8×10^{-10}	3.8×10^{-9}	1.0×10^{-9}
	k_a, M^{-1} s^{-1}	-	-	2.1×10^{6}	4.2×10^{7}	1.3×10^{7}	3.3×10^{5}
	k_d, s^{-1}	-	-	1.0×10^{-2}	7.7×10^{-3}	5.0×10^{-2}	3.3×10^{-4}
13	K_D, M	-	4.8×10^{-9}	1.7×10^{-9}	1.9×10^{-13}	4.5×10^{-11}	2.0×10^{-9}
	k_a, M^{-1} s^{-1}	-	1.8×10^{6}	1.2×10^{6}	6.6×10^{7}	1.2×10^{7}	4.0×10^{6}
	k_d, s^{-1}	-	8.7×10^{-3}	2.0×10^{-3}	1.3×10^{-5}	5.3×10^{-4}	7.9×10^{-3}
14	K_D, M	4.3×10^{-9}	3.9×10^{-10}	1.7×10^{-10}	5.8×10^{-10}	5.0×10^{-9}	4.5×10^{-10}
	k_a, M^{-1} s^{-1}	2.3×10^{6}	2.1×10^{7}	5.5×10^{6}	1.7×10^{8}	2.8×10^{7}	1.5×10^{6}
	k_d, s^{-1}	1.0×10^{-2}	8.2×10^{-3}	9.0×10^{-4}	1.0×10^{-1}	1.4×10^{-1}	1×10^{-8}
15	K_D, M	-	-	4.1×10^{-12}	3.4×10^{-10}	3.2×10^{-9}	8.3×10^{-10}
	k_a, M^{-1} s^{-1}	-	-	4.5×10^{6}	1.9×10^{7}	3.4×10^{6}	4.6×10^{5}
	k_d, s^{-1}	-	-	1.8×10^{-5}	6.4×10^{-3}	1.1×10^{-2}	3.8×10^{-4}
16	K_D, M	-	1.9×10^{-10}	6.6×10^{-10}	1.7×10^{-10}	1.1×10^{-9}	9.1×10^{-10}
	k_a, M^{-1} s^{-1}	-	4.9×10^{7}	1.1×10^{8}	8.8×10^{8}	3.6×10^{7}	1.2×10^{7}
	k_d, s^{-1}	-	9.3×10^{-3}	7.1×10^{-2}	1.5×10^{-1}	4.1×10^{-2}	1.1×10^{-2}
17	K_D, M	2.4×10^{-9}	1.0×10^{-9}	5.9×10^{-8}	1.3×10^{-9}	-	8.7×10^{-9}
	k_a, M^{-1} s^{-1}	2.7×10^{6}	2.6×10^{7}	2.4×10^{6}	2.0×10^{8}	-	2.5×10^{6}
	k_d, s^{-1}	6.6×10^{-3}	2.6×10^{-2}	1.4×10^{-1}	2.6×10^{-1}	-	2.2×10^{-2}

[a]The SPR experiments were repeated at least twice, and the standard deviation did not exceed 1.4 fold of the value.

structures is elusive due to the highly empirical nature of the observed data and its complexity. Methods to dissect the quantifiable interactions into experiment-related and intrinsic properties of a system are needed to contribute to improved quantitative structure−activity relationship correlations and more rational structural design of ligands with desired properties.

Studying chemical and enzyme-catalyzed reactions under various conditions, accounting for solvent polarity, viscosity, and acid/base concentrations is a classical approach to reveal the reaction mechanism. A similar approach can be applied to biomolecular interactions, aiming to identify crucial structural features of functional groups for complexation and their roles.[33,34] However, the structural diversity, nature, and complexity of protein−ligand interactions make the interpretation of experimental data ambiguous.

It was possible to quantify intrinsic association rate constants using eq 4. As expected, for a given interaction the value of k_a^{intr}

DOI: 10.1021/acs.jmedchem.7b01408
J. Med. Chem. 2018, 61, 2292−2302

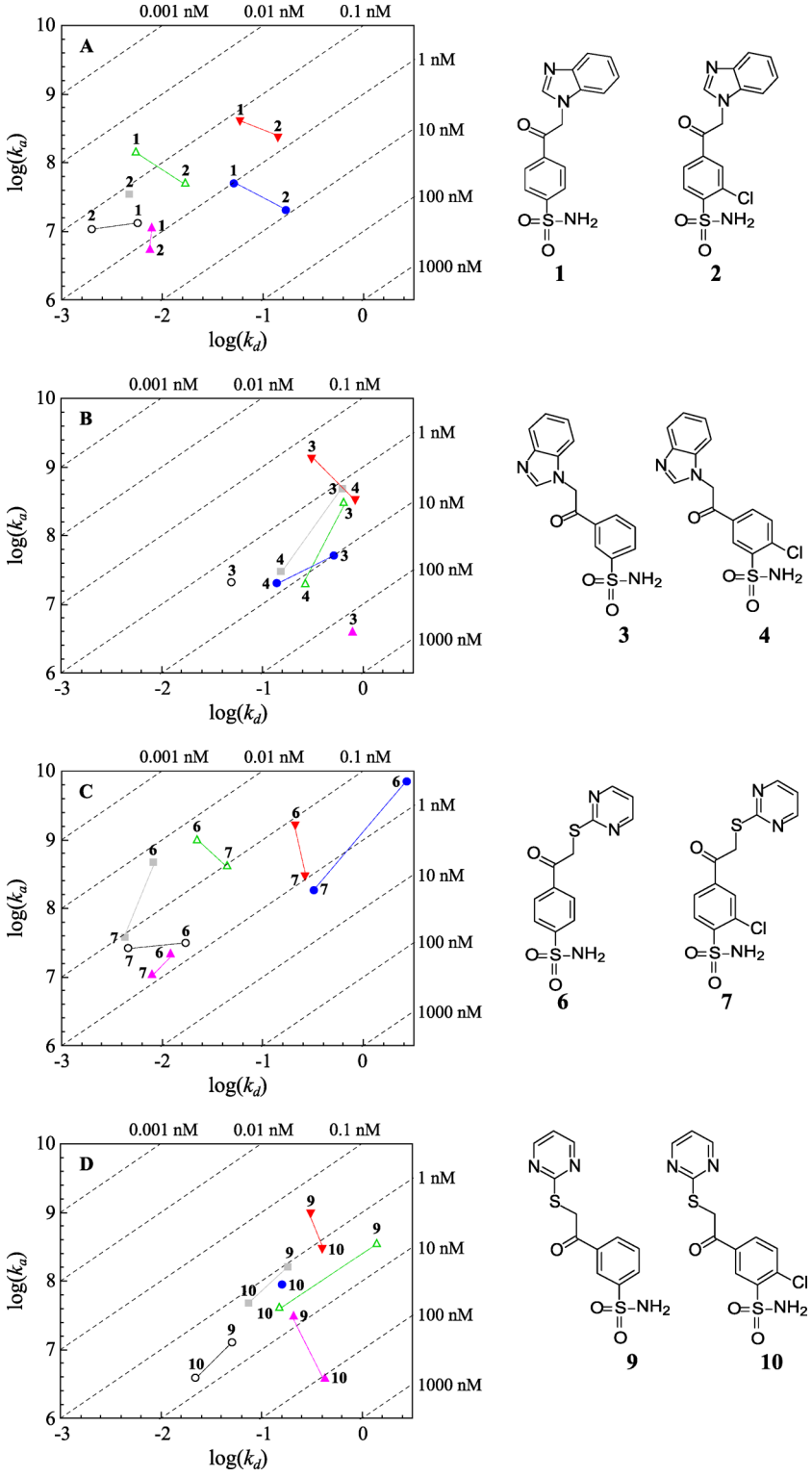

Figure 6. Interaction kinetic plots based on intrinsic association and dissociation rate constants for *ortho*-substituted sulfonamides with CA I (magenta filled triangle), CA II (gray filled square), CA VII (green open triangle), CA IX (red filled down-pointing triangle), CA XII (blue filled circle), and CA XIII (black open circle).

after taking into account fractional concentrations of interacting species is significantly higher than the maximal observed k_a^{obs}. Comparison of the observed and intrinsic association rates shows that for this series of compounds, the difference may reach 1−4 orders of magnitude. If the structure−activity analysis of the interaction kinetics is performed by using the observed association rates, the error may be more than 1000-fold and the compounds may be ranked in a wrong order, assigning the observed gain of the interaction potency to wrong structural changes. Therefore, it is important to determine the intrinsic rates for any protein−ligand binding system where binding-linked protonation events occur either for the protein or for the ligand.

Interestingly enough, sulfonamides are generally considered to be "slow" ligands, with second-order rate constants for the

DOI: 10.1021/acs.jmedchem.7b01408
J. Med. Chem. 2018, 61, 2292−2302

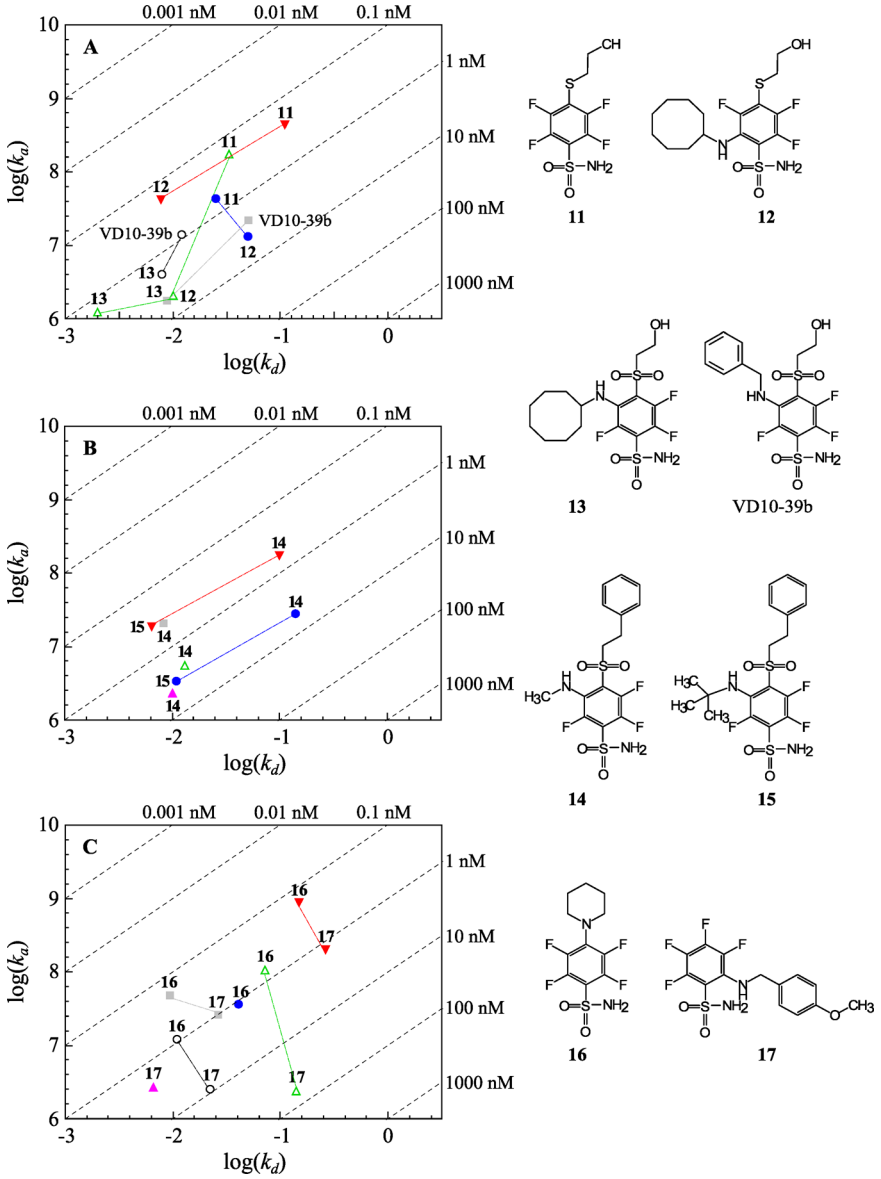

Figure 7. Interaction kinetic plots based on intrinsic association and dissociation rate constants for fluorinated benzenesulfonamide compounds with CA I (magenta filled triangle), CA II (gray filled square), CA VII (green open triangle), CA IX (red filled down-pointing triangle), CA XII (blue filled circle), and CA XIII (black open circle).

association below expected from a small charged molecule that encounter a target with an oppositely charged ion located in a relatively large active site cavity, facilitating efficient docking. The unexpectedly slow association is here explained by the difference between the total concentration of various ligand and protein forms and the active concentration of reactive species. Similar conclusions can be drawn for other families of proteins and ligand chemotypes. It is important that the proposed conceptualization is valid for various types of prereaction equilibria, for example, between various protein conformations, like the conformational selection model.[35,36]

We suggest that the observed experimental parameters should not be directly translated into a structure−activity relationship. The observed gain in inhibitor potency after chemical modification can be attributed to an increase in pK_a value for ionizable pharmacophore and corresponding jump in observed affinity instead of to an improvement in the interaction network.[28] Thus, quantification of intrinsic interaction parameters, including ΔH^{intr}, ΔS^{intr}, K_D^{intr}, k_a^{intr} and k_d^{intr} provide a better link between the ligand structure and its activity toward the target. In addition, knowing the intrinsic parameters allows one to predict the desired activity of a compound in a certain environment and how it depends on pH or ionic strength. Such knowledge is beneficial when the target compartmentalization is of issue.[33]

In this work, we demonstrated the possibility of quantifying intrinsic interaction kinetic parameters for biomolecular interactions using convenient macroscopic techniques. Intrinsic energies and rate constants can reveal the mechanism of the interaction, and are consequently useful for describing genuine characteristics of the interaction, disregarding the influence of coupled reactions and various equilibria that may occur in a target-ligand system. Their evaluation is crucial for a deep characterization of important activity probes, e.g. potential pharmaceuticals in the later stages of their development. As the affinity will have the same pH dependency as the association rate constants, it can be hypothesized that it is possible to design an inhibitor that has an

DOI: 10.1021/acs.jmedchem.7b01408
J. Med. Chem. 2018, 61, 2292−2302

optimal affinity for a particular isoform at a defined pH, which could be beneficial for physiological selectivity.

CONCLUSION

It is important to distinguish the *intrinsic* from the *observed* interaction kinetic parameters when studying any chemical ligand–protein interaction. Binding-linked protonation reactions diminished the association rate of sulfonamide binding to carbonic anhydrases. It was therefore important to calculate the intrinsic association rate constants, based on the available fractions of reacting species. The observed and intrinsic dissociation rates did not differ and thus the intrinsic dissociation rates could be observed experimentally, but not the association rates. Intrinsic association rates are consistent with the diffusion-limited first order rate constants. Structure–kinetics relationships of a series of substituted benzenesulfonamides to several CA isoforms provided insights explaining the high affinities and selectivities of some compounds toward some CA isoforms.

EXPERIMENTAL SECTION

Proteins and Ligands. Carbonic anhydrase II, IX, and XIII were expressed and purified as previously described.[16,37,38] The synthesis, chemical structural characterization, and purity of the compounds used in this study has been previously described: **8** (compound E67) in Čapkauskaitė et al.,[39] compound VD10-39b in Dudutienė et al.,[29] **3** (compound E11–37) in Zubrienė et al.[24] All compounds had a purity higher than 98%, as judged by HPLC analysis. Acetazolamide and *para*-methyl benzensulfonamide were from Sigma Chemical Co. Purchased inhibitors were used without further purification.

Surface Plasmon Resonance Biosensor Analysis. Time-resolved interaction kinetic assays were performed with Biacore S51 or Biacore T200 surface plasmon resonance biosensor instruments (GE Healthcare, Uppsala, Sweden). All experiments were performed at 25 °C.

Sensor surface preparation. Proteins were immobilized on CM5 sensor chips (GE Healthcare, Uppsala, Sweden) using a standard amine coupling procedure. The carboxymethyl dextran matrix of the sensor chip was activated with 0.1 M *N*-hydroxysuccinimide (NHS) and 0.4 M 1-ethyl-3-(3-(dimethylamino)propyl) carbodiimidehydrochloride (EDC) at a flow rate of 10 μL min^{-1} for 7 min.

The immobilization was performed with 100 μg mL^{-1} CA II in 10 mM sodium acetate at pH 5.0, 200 μg mL^{-1} CA IX in 10 mM sodium acetate at pH 4.5, and 200 μg mL^{-1} CA XIII in 10 mM sodium acetate at pH 5.0. Unreacted activated groups of the dextran matrix were deactivated by injection of 1 M ethanolamine hydrochloride (pH 8.5) for 10 min. It was performed using phosphate buffer saline (PBS, 10 mM phosphate, 150 mM NaCl, pH 7.4) as running buffer.

Interaction Kinetic Analysis. Interaction assays were performed in running buffers consisting of 50 mM sodium acetate at pH 5.5, sodium phosphate at pH range from 6 to 8, and tris(hydroxymethyl)-aminomethane hydrochloride (Tris-HCl) at pH 8.5 and 9.0, all supplemented with 100 mM NaCl and 2% (v/v) DMSO. Compounds were prepared from 10 mM DMSO stock solutions, diluted in the running buffer without DMSO. A flow rate of 30 μL min^{-1} was used, and the association was monitored for 60 s, while the dissociation time was selected with respect to the complex stability.

Theoretical binding constants were calculated for every pH, using the equation for intrinsic binding constant. Compounds were injected in a 2-fold dilution series, starting at a concentration 10 times higher than the expected K_D value for each protein–ligand combination and pH value. All concentration series consisted of 6 injections of analyte and 2 blank injections of running buffer.

Acquired sensorgrams were double-referenced against an intact surface and an average of two blank injections. They were solvent corrected and analyzed using Biacore T100 v.2.0, Biacore T200 v.1.0 and BIAevaluation v.3.0 software (GE Healthcare, Uppsala, Sweden). Global analysis of sensorgrams at multiple concentrations was performed using a standard reversible 1:1 Langmuir interaction model.

Data Processing. Instant JChem 6.1.3, 2013, ChemAxon (http://www.chemaxon.com) was used for structure database management, search and prediction. QtiPlot, GNUplot, and Inkscape were used to prepare the figures. GNUplot, R, and Excel were used for regression analyses and data plotting, except the interaction kinetic analysis as described in the Interaction Kinetic Analysis section above.

ASSOCIATED CONTENT

Supporting Information

The Supporting Information is available free of charge on the ACS Publications website at DOI: 10.1021/acs.jmedchem.7b01408.

SMILES strings for studied compounds and association, dissociation rate constants and equilibrium constants with human CAs (CSV)

AUTHOR INFORMATION

Corresponding Author

*E-mail: matulis@ibt.lt, phone: +37052234364, fax: +37052234367.

ORCID

U. Helena Danielson: 0000-0003-2728-0340

Daumantas Matulis: 0000-0002-6178-6276

Author Contributions

‖Contributed equally to this work

Notes

The authors declare no competing financial interest.

ACKNOWLEDGMENTS

This research was funded by grant no. S-MIP-17-87 from the Research Council of Lithuania, the Swedish Research Council (VR) grant no. D0571301, and Carl Tryggers Stiftelse. The authors also acknowledge the COST projects CA15126, CA15135, CM1406, and CM1407. The authors are thankful to Dr. Helena Nordström (Sci-Life Lab, Uppsala University, Uppsala, Sweden) for providing access to Biacore T200 instrument.

ABBREVIATIONS USED

AZM - acetazolamide; CA - carbonic anhydrase; FTSA - fluorescent thermal shift assay; k_a^{intr} - intrinsic association rate constant; k_a^{obs} - observed association rate constant; k_d^{intr} - intrinsic dissociation rate constant; K_D^{intr} - intrinsic equilibrium dissociation constant; k_d^{obs} - observed dissociation rate constant; K_D^{obs} - observed equilibrium dissociation constant; p-MBS - *para*-methyl benzensulfonamide; SA - sulfonamide; SPR - surface plasmon resonance

REFERENCES

(1) Supuran, C. T. Structure and function of carbonic anhydrases. *Biochem. J.* **2016**, *473*, 2023–2032.

(2) McKenna, R.; Frost, S. C. Overview of the carbonic anhydrase family. *Subcell. Biochem.* **2014**, *75*, 3–5.

(3) Pastorek, J.; Pastorekova, S. Hypoxia-induced carbonic anhydrase IX as a target for cancer therapy: from biology to clinical use. *Semin. Cancer Biol.* **2015**, *31*, 52–64.

(4) Tafreshi, N. K.; Lloyd, M. C.; Bui, M. M.; Gillies, R. J.; Morse, D. L. Carbonic anhydrase IX as an imaging and therapeutic target for tumors and metastases. *Subcell. Biochem.* **2014**, *75*, 221–254.

(5) Smirnovienė, J.; Smirnovas, V.; Matulis, D. Picomolar inhibitors of carbonic anhydrase: Importance of inhibition and binding assays. *Anal. Biochem.* **2017**, *522*, 61–72.

DOI: 10.1021/acs.jmedchem.7b01408
J. Med. Chem. 2018, 61, 2292–2302

(6) Taylor, P. W.; King, R. W.; Burgen, A. S. Influence of pH on the kinetics of complex formation between aromatic sulfonamides and human carbonic anhydrase. *Biochemistry* **1970**, *9*, 3894−3902.
(7) Fisher, S. Z.; Aggarwal, M.; Kovalevsky, A. Y.; Silverman, D. N.; McKenna, R. Neutron diffraction of acetazolamide-bound human carbonic anhydrase II reveals atomic details of drug binding. *J. Am. Chem. Soc.* **2012**, *134*, 14726−14729.
(8) Gaspari, R.; Rechlin, C.; Heine, A.; Bottegoni, G.; Rocchia, W.; Schwarz, D.; Bomke, J.; Gerber, H.-D.; Klebe, G.; Cavalli, A. Kinetic and structural insights into the mechanism of binding of sulfonamides to human carbonic anhydrase by computational and experimental studies. *J. Med. Chem.* **2016**, *59*, 4245−4256.
(9) Talibov, V. O.; Linkuvienė, V.; Matulis, D.; Danielson, U. H. Kinetically selective inhibitors of human carbonic anhydrase isozymes I, II, VII, IX, XII, and XIII. *J. Med. Chem.* **2016**, *59*, 2083−2093.
(10) Morkūnaitė, V.; Gylytė, J.; Zubrienė, A.; Baranauskienė, L.; Kišonaitė, M.; Michailovienė, V.; Juozapaitienė, V.; Todd, M. J.; Matulis, D. Intrinsic thermodynamics of sulfonamide inhibitor binding to human carbonic anhydrases I and II. *J. Enzyme Inhib. Med. Chem.* **2015**, *30*, 204−211.
(11) Kasiliauskaitė, A.; Časaitė, V.; Juozapaitienė, V.; Zubrienė, A.; Michailovienė, V.; Revuckienė, J.; Baranauskienė, L.; Meškys, R.; Matulis, D. Thermodynamic characterization of human carbonic anhydrase VB stability and intrinsic binding of compounds. *J. Therm. Anal. Calorim.* **2016**, *123*, 2191−2200.
(12) Kazokaitė, J.; Milinavičiūtė, G.; Smirnovienė, J.; Matulienė, J.; Matulis, D. Intrinsic binding of 4-substituted-2,3,5,6-tetrafluorobenezenesulfonamides to native and recombinant human carbonic anhydrase VI. *FEBS J.* **2015**, *282*, 972−983.
(13) Pilipuitytė, V.; Matulis, D. Intrinsic thermodynamics of trifluoromethanesulfonamide and ethoxzolamide binding to human carbonic anhydrase VII. *J. Mol. Recognit.* **2015**, *28*, 166−172.
(14) Jogaitė, V.; Zubrienė, A.; Michailovienė, V.; Gylytė, J.; Morkūnaitė, V.; Matulis, D. Characterization of human carbonic anhydrase XII stability and inhibitor binding. *Bioorg. Med. Chem.* **2013**, *21*, 1431−1436.
(15) Baranauskienė, L.; Matulis, D. Intrinsic thermodynamics of ethoxzolamide inhibitor binding to human carbonic anhydrase XIII. *BMC Biophys.* **2012**, *5*, 12.
(16) Linkuvienė, V.; Matulienė, J.; Juozapaitienė, V.; Michailovienė, V.; Jachno, J.; Matulis, D. Intrinsic thermodynamics of inhibitor binding to human carbonic anhydrase IX. *Biochim. Biophys. Acta, Gen. Subj.* **2016**, *1860*, 708−718.
(17) Patching, S. G. Surface plasmon resonance spectroscopy for characterisation of membrane protein-ligand interactions and its potential for drug discovery. *Biochim. Biophys. Acta, Biomembr.* **2014**, *1838*, 43−55.
(18) Meyer-Almes, F.-J. Kinetic binding assays for the analysis of protein-ligand interactions. *Drug Discovery Today: Technol.* **2015**, *17*, 1−8.
(19) Swinney, D. C. The role of binding kinetics in therapeutically useful drug action. *Curr. Opin. Drug Discov. Dev.* **2009**, *12*, 31−39.
(20) Klebe, G. The use of thermodynamic and kinetic data in drug discovery: decisive insight or increasing the puzzlement? *ChemMedChem* **2015**, *10*, 229−231.
(21) Baker, B. M.; Murphy, K. P. Evaluation of linked protonation effects in protein binding reactions using isothermal titration calorimetry. *Biophys. J.* **1996**, *71* (4), 2049−55.
(22) Zubrienė, A.; Gutkowska, M.; Matulienė, J.; Chaleckis, R.; Michailovienė, V.; Voroncova, A.; Venclovas, C.; Zylicz, A.; Zylicz, M.; Matulis, D. Thermodynamics of radicicol binding to human Hsp90 alpha and beta isoforms. *Biophys. Chem.* **2010**, *152*, 153−163.
(23) Kišonaitė, M.; Zubrienė, A.; Čapkauskaitė, E.; Smirnov, A.; Smirnovienė, J.; Kairys, V.; Michailovienė, V.; Manakova, E.; Gražulis, S.; Matulis, D. Intrinsic thermodynamics and structure correlation of benzenesulfonamides with a pyrimidine moiety binding to carbonic anhydrases I, II, VII, XII, and XIII. *PLoS One* **2014**, *9*, e114106.
(24) Zubrienė, A.; Čapkauskaitė, E.; Gylytė, J.; Kišonaitė, M.; Tumkevičius, S.; Matulis, D. Benzenesulfonamides with benzimidazole moieties as inhibitors of carbonic anhydrases I, II, VII, XII and XIII. *J. Enzyme Inhib. Med. Chem.* **2014**, *29*, 124−131.
(25) Čapkauskaitė, E.; Baranauskienė, L.; Golovenko, D.; Manakova, E.; Gražulis, S.; Tumkevičius, S.; Matulis, D. Indapamide-like benzenesulfonamides as inhibitors of carbonic anhydrases I, II, VII, and XIII. *Bioorg. Med. Chem.* **2010**, *18*, 7357−7364.
(26) Čapkauskaitė, E.; Zubrienė, A.; Baranauskienė, L.; Tamulaitienė, G.; Manakova, E.; Kairys, V.; Gražulis, S.; Tumkevičius, S.; Matulis, D. Design of [(2-pyrimidinylthio)acetyl]benzenesulfonamides as inhibitors of human carbonic anhydrases. *Eur. J. Med. Chem.* **2012**, *51*, 259−270.
(27) Dudutienė, V.; Zubrienė, A.; Smirnov, A.; Gylytė, J.; Timm, D.; Manakova, E.; Gražulis, S.; Matulis, D. 4-Substituted-2,3,5,6-tetrafluorobenzenesulfonamides as inhibitors of carbonic anhydrases I, II, VII, XII, and XIII. *Bioorg. Med. Chem.* **2013**, *21*, 2093−2106.
(28) Dudutienė, V.; Matulienė, J.; Smirnov, A.; Timm, D. D.; Zubrienė, A.; Baranauskienė, L.; Morkūnaitė, V.; Smirnovienė, J.; Michailovienė, V.; Juozapaitienė, V.; Mickevičiūtė, A.; Kazokaitė, J.; Bakšytė, S.; Kasiliauskaitė, A.; Jachno, J.; Revuckienė, J.; Kišonaitė, M.; Pilipuitytė, V.; Ivanauskaitė, E.; Milinavičiūtė, G.; Smirnovas, V.; Petrikaitė, V.; Kairys, V.; Petrauskas, V.; Norvaišas, P.; Lingė, D.; Gibieža, P.; Čapkauskaitė, E.; Zakšauskas, A.; Kazlauskas, E.; Manakova, E.; Gražulis, S.; Ladbury, J. E.; Matulis, D. Discovery and characterization of novel selective inhibitors of carbonic anhydrase IX. *J. Med. Chem.* **2014**, *57*, 9435−9446.
(29) Dudutienė, V.; Zubrienė, A.; Smirnov, A.; Timm, D. D.; Smirnovienė, J.; Kazokaitė, J.; Michailovienė, V.; Zakšauskas, A.; Manakova, E.; Gražulis, S.; Matulis, D. Functionalization of fluorinated benzenesulfonamides and their inhibitory properties toward carbonic anhydrases. *ChemMedChem* **2015**, *10*, 662−687.
(30) Karlsson, R.; Katsamba, P.; Nordin, H.; Pol, E.; Myszka, D. Analyzing a kinetic titration series using affinity biosensors. *Anal. Biochem.* **2006**, *349*, 136−147.
(31) Karlsson, R. Affinity analysis of non-steady-state data obtained under mass transport limited conditions using BIAcore technology. *J. Mol. Recognit.* **1999**, *12*, 285−292.
(32) Renaud, J.-P.; Chung, C.-w.; Danielson, U. H.; Egner, U.; Hennig, M.; Hubbard, R. E.; Nar, H. Biophysics in drug discovery: impact, challenges and opportunities. *Nat. Rev. Drug Discovery* **2016**, *15*, 679−698.
(33) Dominguez, J. L.; Christopeit, T.; Villaverde, M. C.; Gossas, T.; Otero, J. M.; Nystrom, S.; Baraznenok, V.; Lindstrom, E.; Danielson, U. H.; Sussman, F. Effect of the protonation state of the titratable residues on the inhibitor affinity to BACE-1. *Biochemistry* **2010**, *49*, 7255−7263.
(34) Sussman, F.; Villaverde, M. C.; Dominguez, J. L.; Danielson, U. H. On the active site protonation state in aspartic proteases: implications for drug design. *Curr. Pharm. Des.* **2013**, *19*, 4257−4275.
(35) Eigen, M. New looks and outlooks on physical enzymology. *Q. Rev. Biophys.* **1968**, *1*, 3−33.
(36) Boehr, D. D.; Nussinov, R.; Wright, P. E. The role of dynamic conformational ensembles in biomolecular recognition. *Nat. Chem. Biol.* **2009**, *5*, 789−796.
(37) Cimmperman, P.; Baranauskienė, L.; Jachimovičiūtė, S.; Jachno, J.; Torresan, J.; Michailovienė, V.; Matulienė, J.; Sereikaitė, J.; Bumelis, V.; Matulis, D. A quantitative model of thermal stabilization and destabilization of proteins by ligands. *Biophys. J.* **2008**, *95*, 3222−3231.
(38) Sūdžius, J.; Baranauskienė, L.; Golovenko, D.; Matulienė, J.; Michailovienė, V.; Torresan, J.; Jachno, J.; Sukackaitė, R.; Manakova, E.; Gražulis, S.; Tumkevičius, S.; Matulis, D. 4-[N-(substituted 4-pyrimidinyl)amino]benzenesulfonamides as inhibitors of carbonic anhydrase isozymes I, II, VII, and XIII. *Bioorg. Med. Chem.* **2010**, *18*, 7413−7421.
(39) Čapkauskaitė, E.; Zubrienė, A.; Smirnov, A.; Torresan, J.; Kišonaitė, M.; Kazokaitė, J.; Gylytė, J.; Michailovienė, V.; Jogaitė, V.; Manakova, E.; Gražulis, S.; Tumkevičius, S.; Matulis, D. Benzenesulfonamides with pyrimidine moiety as inhibitors of human carbonic anhydrases I, II, VI, VII, XII, and XIII. *Bioorg. Med. Chem.* **2013**, *21*, 6937−6947.

DOI: 10.1021/acs.jmedchem.7b01408
J. Med. Chem. 2018, 61, 2292−2302